An Experimental Technique for Measurement of Injector Spray Mixing

W. H. NURICK* AND S. D. CLAPP†
Rocketdyne, A Division of North American Rockwell Corporation, Canoga Park, Calif.

Nomenclature

A = area
c^* = characteristic velocity
C_D = drag coefficient
D = droplet diameter
l,n = V_{DY}/V_Z and V_{DZ}/V_Z, respectively
t = time
V = velocity
$\dot{w}$ = flow rate
Y = radial distance
α = V_Y/V_Z
ρ = density

Subscripts

D = droplet
dist = distribution
g = gas
i = ith stream tube
T = total injected
theo = theoretical
t_i = throat for the ith tube
Y, Z = radial and axial directions, respectively

Introduction

PRIOR studies[1-7] have related liquid-rocket spray characteristics to injector mechanical and hydraulic parameters and/or combustion efficiencies from hot firings, i.e., to measured performance, but none has predicted combustion efficiency from spray measurements. This Note presents a technique that combines spray data obtained with nonreactive propellant simulants with an analytical model to predict the loss in combustion efficiency due to nonuniformities in the propellant mixture ratio distribution. Efficiencies thus predicted are compared with hot-firing results.

The combustion chamber is considered to be divided into a primary mixing zone that includes the initial combustion region and that terminates when the gas velocity has essentially turned the spray in the axial direction, and a secondary zone, wherein turbulent vaporization and combustion occur within stream tubes, but with no thermal or mass transfer between stream tubes.

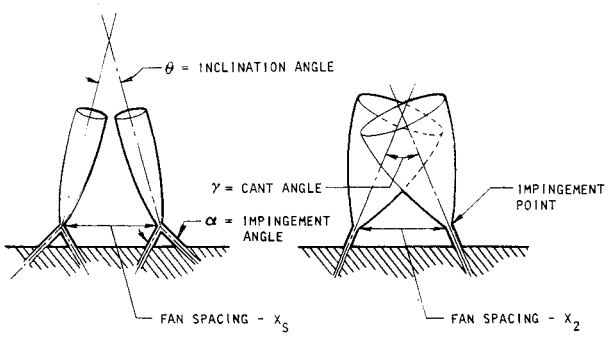

Fig. 1 Illustration of the injector variables for a like-impinging doublet injector design.

Received April 28, 1969; revision received July 23, 1969. The major portion of the data presented in this paper was obtained under AFRPL Contract AF04(611)-67-C-0081.

* Principal Scientist. Member AIAA.

† Manager. Member AIAA.

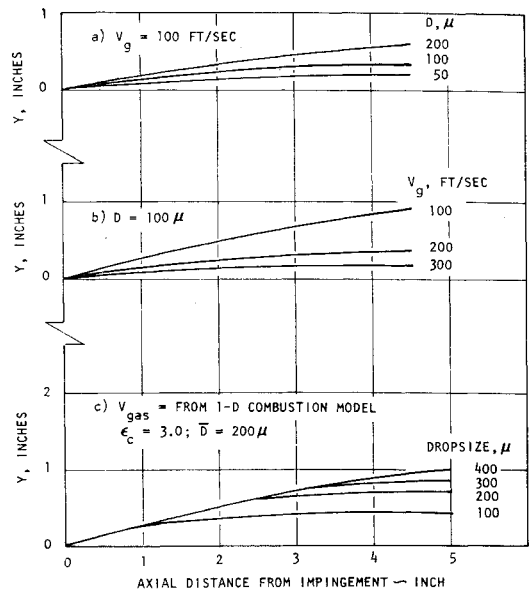

Fig. 2 Trajectories of individual droplets of various sizes contained in a spray field having a mass medium dropsize of 200 *M*.

Primary mixing is induced by impingement of the propellant streams (Fig. 1). If the spray is assumed to be composed of droplets whose flight paths are not influenced by the surrounding droplets, then the equation of motion is

$$dV_D/dt = \beta|\mathbf{V}_g - \mathbf{V}_D|(\mathbf{V}_g - \mathbf{V}_D) \quad (1)$$

where $\beta = 3C_D\rho_g/4\rho_D D$. The integral solution is[9]:

$$Y = \int_0^Z \frac{V_{ZD} + \int_0^Z \xi\beta V_Z(\alpha - l)dz}{V_{ZD} + \int_0^Z \xi\beta V_Z \dfrac{(1-n)}{n} dz} dz \quad (2)$$

where $\xi \equiv [(1-n)^2 + (\alpha - l)^2]^{1/2}$. Solution of Eq. (2) requires knowledge of the initial velocity and direction of the droplets. A spray fan spreads at about the same angle as the initial impingement angle of the jets. Consequently, some mass-weighted average trajectory should be utilized to represent the effective initial angle of the entire spray. For the 30° half-angle impinging jets used in this study, 15° was used as a good approximation of a mass-weighted average drop trajectory angle.

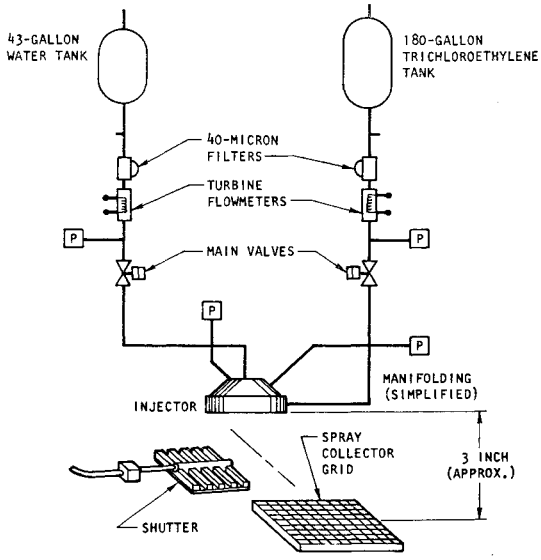

Fig. 3 Schematic diagram of the flow system.

Table 1 Like-on-like, doublet injectors[a]

Injector No.	Number of elements	Fan spacing,[b] χ_s, in.	Orifice diameters, in. D_o–D_f	Cant angle, γ, deg
1	100	0.00	0.033–0.026	0
2	100	0.35		0
3	6	0.00	0.136–0.1065	0
4	6	0.15		0
5	6	0.35		0
6	6	0.08		24
7	6	0.00		41
8	6	0.00	0.182–0.147	0

[a] Total included impingement angle is 60°.
[b] Spacing between fans is the distance between the adjacent oxidizer and fuel element.

Typical droplet trajectories are shown in Fig. 2. The trajectories in Fig. 2c are based on gas velocities predicted from a one-dimensional, vaporization-rate limited combustion model and are representative of those in a combustion chamber. The distance required to turn the sprays to the axial direction is on the order of 3 in., and the mass mean radial displacement is about $\frac{2}{3}$ in.

It should be noted that the Y (radial) displacements given in Eq. (2) and plotted in Fig. 2 are overestimated because interaction between droplets is neglected; thus, the indicated axial distances required for turning are conservative.

A stream-tube analysis[8,10] was used to predict the loss in performance due to the nonuniformities in mass and mixture ratio distributions at the end of the primary mixing zone. In this analysis, the flow in the secondary zone is divided into stream tubes of equal flow area. For each tube, complete vaporization occurs in the combustion chamber and the product gas then expands isentropically through the nozzle. It is assumed that no thermal or chemical intertube mixing occurs, and that pressure continuity is maintained at each transverse station in the nozzle. Chamber pressure, throat area, contraction ratio, and propellant distribution are specified. The static pressure at the throat and the total propellant flow rate are determined by an iteration process.

The result of this analysis, in terms of c^* efficiency, is

$$(\eta_{c^*})_{\text{dist}} = 100 \sum_i [(w_i/w_T)c^*_i(A_{t_i}/A_i^*)]/c^*_{\text{theo}_i} \quad (3)$$

The A_{t_i}/A_i^* factor accounts for the shift in the location of the sonic point due to changes in the specific heat ratio.

Table 2 Hot-firing results

Injector No.	L^*, in.	Mixture ratio	η_{c^*}	Injector, in.	L^*, in.	Mixture ratio	η_{c^*}
1	10	1.05	0.93	5	25	2.07	0.56
		1.88	0.94			2.82	0.58
		1.06	0.97			2.78	0.58
2	25	2.05	0.96			1.21	0.64
		1.10	0.97	7	10	1.95	0.65
		2.03	0.97			2.75	0.69
		2.92	0.98			1.12	0.75
3	25	3.06	0.96		25	2.01	0.82
		0.96	0.69			3.01	0.84
	38	1.03	0.77			1.05	0.89
		2.05	0.77		56	2.04	0.98
		1.98	0.79			3.11	0.93
		2.86	0.84			1.03	0.96
		0.98	0.84	8	25	2.05	0.79
	56	1.99	0.84			2.94	0.80
		2.95	0.90			1.03	0.84
4	25	2.88	0.65		56	2.04	0.90
		2.05	0.66			2.98	0.90
		1.07	0.77			1.04	0.91

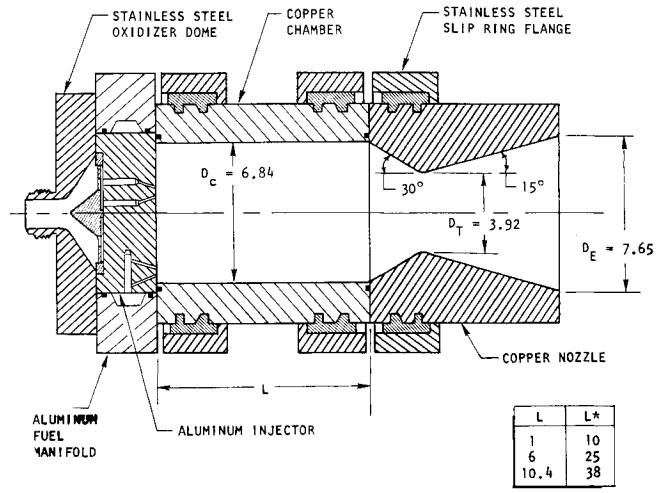

Fig. 4 Cross-sectional view of typical assembled engine used in hot-firing experiments.

Experimental Equipment and Techniques

The objective of the cold-flow tests was to determine the mass and mixture ratio distributions at the end of the primary mixing region. Trichloroethylene and water were used as propellant simulants, on the basis of their immiscibility, ease of handling, and similarity of physical properties to those of N_2O_4 and N_2H_4-UDMH (50-50). Figure 3 depicts the flow system and the collection grid, in which squared-end, 0.25-in. tubes are arranged in a 29 × 29 matrix. The squared ends permit adjacent tubes to touch over their perimeters, thereby maximizing the sampling area. The shutters, which deflect the spray away from the collector until steady-flow conditions are attained, are employed to reduce start-and-stop transient errors. From the collection grid, the tubes slant outward to a 7- by 7-ft base in which 841 pyrex tubes are mounted (one for each sampling station). Capacity of each pyrex tube is 650 cm³.

Total flow rate in the cold-flow tests was 22.1 lb/sec, corresponding to the theoretical flowrate for rocket operation at the 5000-lb-thrust level. Each injector was cold-flow tested at three to five different mixture ratios. Flow durations were 10–15 sec. All tests were conducted with the injector centered above the collector at a distance of 2.75 in. from

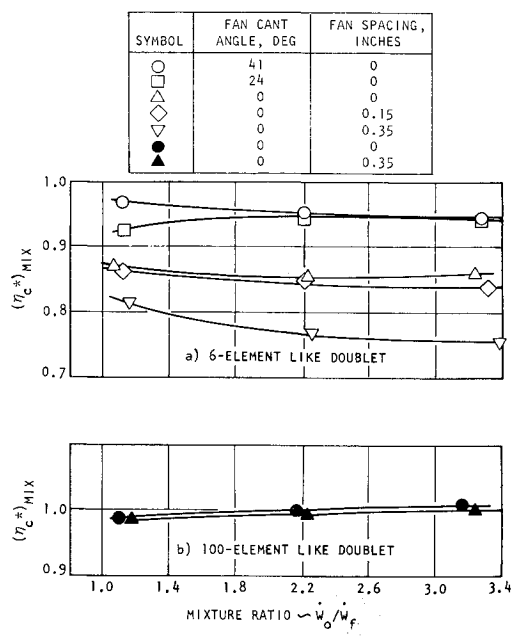

Fig. 5 Cold-flow mixing results for several like-doublet injector designs, 2.75 in. from impingement point.

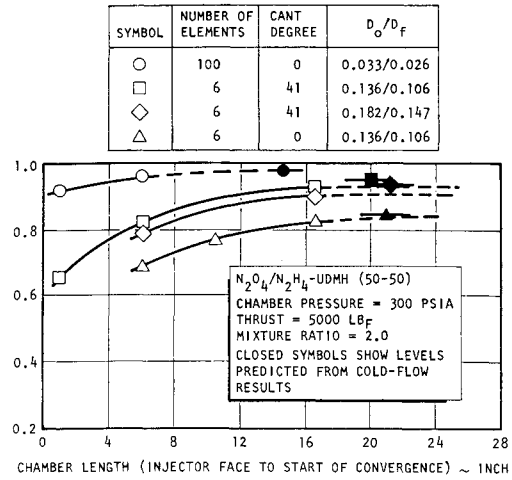

Fig. 6 Effect of chamber length on c^* efficiency for several like-doublet injector design and comparison with cold-flow predictions.

the jet impingment point. This distance was selected because the analytical model describing droplet trajectories in the primary mixing zone, as well as some preliminary experimental data, indicated that this approximated the extent of the primary propellant mixing region during combustion. Since, in a firing, the combustion chamber walls limit the expanding propellant spray field, the cold-flow data reduction computer program was written so that liquids collected outside the physical chamber diameter (6.84 in.) were considered to have been collected in the nearest tube within the chamber radius. (The collector grid measured 7.75 in. × 7.75 in.)

The test engine used for the hot firings is shown in Fig. 4. Eight like-on-like doublet injectors were used (Table 1). All were designed for operation at 5000-lb thrust and 300-psia chamber pressure with the N_2O_4/N_2H_4-UDMH (50-50) propellant combination. The three parameters most influential in controlling the spray distribution characteristics of like-impinging injectors are illustrated in Fig. 1. These are the spacing between fans (χ_S and χ_2), the fan inclination angle (θ), and the fan cant angle (γ). Variations in distribution for the 100-element injectors were obtained by varying the fan spacing (χ_S) between the oxidizer and fuel elements, and for the 6-element injectors by varying χ_S and γ. All other injector parameters were kept constant. The impingement angle (α) was 60° in all injectors.

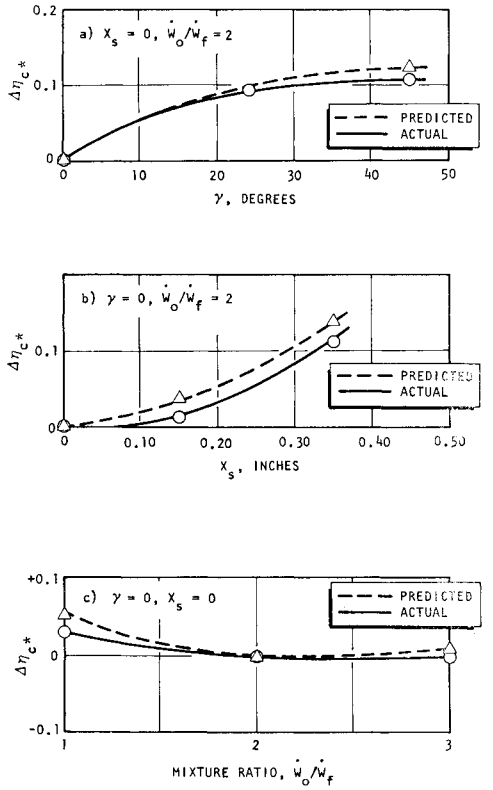

Fig. 7 Comparison between cold-flow-predicted and hot-firing c^* efficiency variations for 6-element, like-doublet injectors.

Results and Discussion

The cold-flow test data (Fig. 5) show that both χ_S and γ significantly affect the predicted c^* efficiencies for the 6-element injectors (which have high thrust per element) but χ_S has no appreciable effect for the 100-element injectors, which yield high efficiencies.

Test firing results are given in Table 2, in terms of corrected c^* efficiency. Since $(1 - \eta_{c*})$ is a measure of the combustion losses incurred as a result of both incomplete vaporization and nonuniform mass and mixture ratio distributions, the values of η_{c*} shown in this table do not reflect mixing losses alone. However, comparisons between injectors designed with the same number of elements and injection ΔP indicate relative trends. The effect of chamber length on η_{c*} is shown in Fig. 6 for four injectors. In all cases, performance increases with increasing length until a maximum level is attained. With the 6-element designs, increasing the cant angle increased performance by about 10% (84 to 94%). Decreasing orifice size (ΔP = const) from the 6-element design to the 100-element design increased performance about 14% (84 to 98%).

Figure 7 compares cold-flow predictions and test-firing results for the 6-element injectors. Over the range of fan cant angle from 0 to 41°, the agreement is within 1% of η_{c*}. For fan spacings (χ_S) of 0 to 0.35 in., the predicted increases in η_{c*} are 2% greater than those actually obtained. This is attributed to the fact that the collection distance should have been somewhat larger for these designs. Correct trends are predicted as mixture ratio is varied, but the predicted c^* efficiencies are about 2% high.

From this study it is concluded that the sampling/collection apparatus developed, when used with appropriately simulated propellants and the mixing-limited, stream-tube analysis described herein, provides a relatively simple means of defining injector design criteria for optimum propellant mixing.

References

[1] Rupe, J. H., "The Liquid Phase Mixing of a Pair of Impinging Streams," Progress Rept. 20-195, Aug. 1953, Jet Propulsion Lab., Pasadena, Calif.

[2] Rupe, J. H., "A Correlation Between the Dynamic Properties of a Pair of Impinging Streams and the Uniformity of Mixture-Ratio Distribution in the Resulting Spray," Progress Rept. 20-209, March 1956, Jet Propulsion Lab., Pasadena, Calif.

[3] Rupe, J. H., "An Experimental Correlation of the Nonreactive Properties of Injection Schemes and Combustion Effects in a Liquid-Propellant Rocket Engine," TR 32-255, July 1965, Jet Propulsion Lab., Pasadena, Calif.

[4] Elverum, G. W. and Morey, T., "Criteria for Optimum Mixture Ratio Distribution Using Several Types of Impinging-Stream Injector Elements," Memo 30-5, Feb. 1959, Jet Propulsion Lab., Pasadena, Calif.

[5] Pieper, J. L., Dean, L. E., and Valentine, R. S., "Mixture Ratio Distribution—Its Impact on Rocket Thrust Chamber Performance," *Journal of Spacecraft and Rockets*, Vol. 4, No. 6, June 1967, pp. 786–789.

[6] "Study of Droplet Effects on Steady-State Combustion," TR-66-152, Vol. 2, Aug. 1966, Rocketdyne, a Division of North American Rockwell Corp., Canoga Park, Calif.

[7] Riebling, R. W., "Criteria for Optimum Propellant Mixing in Impinging-Jet Injection Elements," *Journal of Spacecraft and Rockets*, Vol. 4, No. 6, June 1967, pp. 817–819.

[8] Wrobel, J. R., "Some Effects of Gas Stratification upon Choked Nozzle Flows," AIAA Paper 64-266, Washington, D. C., 1964.

[9] Coultas, T. A., "Radial Winds," 5th ICRPG Combustion Conference, Baltimore, Md., Oct. 1968, to be published.

[10] Dickerson, R. A. et al., "Correlation of Spray Injector Parameters With Rocket Engine Performance," TR AFRPL-TR-68-147, June 1968, Air Force Rocket Propulsion Lab.

Comparison of Separate and Integral Spacecraft

ROBERT J. SALKELD*
Los Angeles, Calif.

Nomenclature

C = cost per flight
c = unit cost
g = acceleration of gravity
I = specific impulse
R = (refurbishment plus amortized replacement cost)/unit cost
v = ideal velocity
w = weight
λ = stage structure factor (empty weight less payload/gross weight less payload)

Subscripts

g = gross
i = integral
p = throw payload
s = separate
u = useful payload

Introduction

EXPANSION of manned space activity can be expected to bring about growing requirements for manned spacecraft capable of performing such missions as logistic shuttle, rescue, reconnaissance and inspection, more flexibility and economically than is possible with current available or funded systems. This has been recognized for some time during which many vehicle concepts have been proposed and evaluated. It has come to be generally agreed that such a spacecraft should be inherently capable of aerodynamic maneuvering by being configured for hypersonic lift-to-drag ratios not less than ~1.5 to provide flexibility in landing site selection, to provide horizontal landing capability, and to reduce thermal shield temperatures during re-entry. It is not so generally agreed, however, whether the spacecraft should provide its own capability for space maneuvering including participation in the launch ascent, orbital change, and rendezvous, in the form of an integral propulsion system, or whether such propulsive capability should be provided by a separate expendable stage.

If total "throw" payload is used as the criterion, as is frequently the case because experience to date is predominantly with nonrecoverable and ballistic systems where total "throw" payload is a reasonable criterion, then the separate vehicle concept often appears preferable because of the favorably low structure factor associated with expendable stages. If, however, "useful" payload is used as a criterion, (and this may be a more direct measure of mission capability where much of the "throw" payload must be allocated to aerodynamic lifting and thermal structure), then under many conditions, the integral vehicle concept may be preferable, both from a weight and cost viewpoint. This will be demonstrated by a parametric performance and cost comparison of representative separate and integral spacecraft concepts.

Received July 29, 1969. The author thanks D. W. Cochran, McDonnell Douglas Corporation, who contributed the cost data on which the cost comparisons are based.

* Consultant, 410½ Landfair Avenue, Westwood Village. Member AIAA.

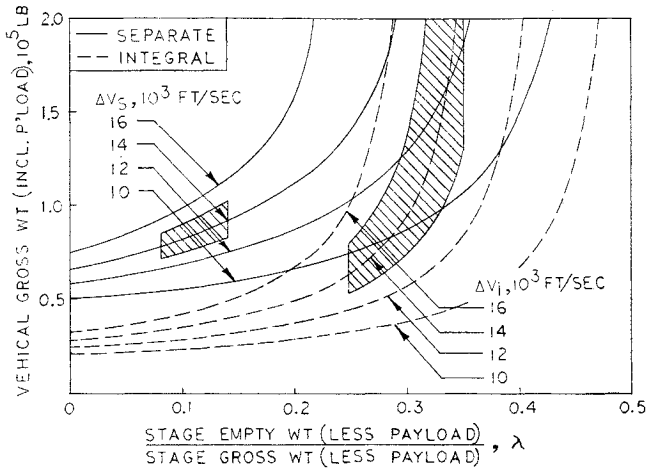

Fig. 1 Gross weight vs structure factor ($I_s = I_i = 450$ sec).

Separate and Integral Vehicle Concepts

The separate vehicle is assumed to consist of a lifting body and an expendable propulsive stage which provides velocity gains necessary for major maneuvers such as optimized participation in launch ascent, orbital change, rendezvous and deorbit. The integral vehicle is assumed to consist of a lifting body containing an integral propulsive capability for maneuvers such as listed above. In general, because of the lower re-entry platform loading of the empty integral spacecraft, that vehicle can utilize radiative thermal shielding, while the nonpropulsive re-entry element of the separate spacecraft would be expected to require an ablative shield.

Since more design data are available for separate spacecraft, that case will be used as the reference in establishing a standard payload applicable to a spectrum of manned near orbit missions. Studies have shown that a wide variety of manned mission requirements can be met with a throw weight in the order of the Titan-IIIC near orbit payload capability of 25,000 lb. Therefore, it will be assumed that $w_p = 25{,}000$ lb.

Useful payload will be defined as including cargo, crew, life support and an appropriate allocation of power and other accessory subsystems. Design data from various sources indicate good general agreement that for a nonpropulsive, medium L/D lifting body having a gross weight of 25,000 lb., the useful payload as here defined will be in the vicinity of 11,000 lb. Thus, assume $w_u = 11{,}000$ lb.

With regard to reasonable values of structure factor, design studies to date seem to justify the following assumed ranges for hydrogen-oxygen propelled vehicles in the size ranges considered: $0.08 \leq \lambda_s \leq 0.14$ and $0.25 \leq \lambda_i \leq 0.35$.

The velocity gain required of each vehicle concept depends on the mission. All missions for this type of spacecraft require launch, however, and except where extensive orbital maneuvers are involved it seems reasonable to assume that almost all the required velocity will be that associated with the latter portions of the ascent to orbit. Launch trajectory optimization studies have shown that the ideal velocity requirements for many cases are about equal for both the separate and integral cases, in the range of 13,000–15,000 fps, which will be the assumed range for both Δv_s and Δv_i.

Thus, the separate and integral concepts can be compared on an essentially equal performance basis without reference to preceding propulsive stages (assuming of course, that